Frequency Response Sensitivity Functions for Helicopter Frequency Domain System Identification

Christopher Tyler Jones NSF Doctoral Fellow, currently at Sikorsky Aircraft Roberto Celi Associate Professor

Alfred Gessow Rotorcraft Center Department of Aerospace Engineering University of Maryland at College Park, Maryland

This paper addresses some aspects of frequency domain based, state space system identification. A frequency response sensitivity function is developed, and applied to the problem of identifying a coupled rotor-fuselage helicopter model from simulated frequency sweep data. This function indicates how sensitive the frequency response of the model is, at every frequency of interest, to perturbations of the model parameters. This information can be used to tailor the identification process by indicating what frequency bands and what inputs are best suited for the identification of a given parameter. The paper also presents expressions for an efficient calculation of the derivatives of this sensitivity function. This enables faster implementations of the frequency response matching problem and of the calculation of accuracy metrics. The sensitivity functions are used to partition an identification problem that covers a very wide frequency band into two identifications over smaller frequency bands. Such frequency-banded identification appears possible, faster, and slightly more accurate for the case studied in the paper. A possible application of this technique is the identification of a coupled rotor-fuselage system from separate low frequency flight tests and higher frequency, rotor wind tunnel tests. The results indicate that the use of the frequency response sensitivity function can help automate some decisions typically left to the analyst's judgment.

Notation

A, B, C	State, control, and output matrices
CR	Cramer-Rao bound
$G(\omega)$	Frequency response matrix
H	Hessian matrix
IS	Parameter insensitivity
J	Objective function for frequency matching
Q	Sensitivity function weighting matrix
W	Coherence weighting matrix
n_i	Number of control inputs
n_o	Number of response outputs
n_{ω}	Number of frequency points at which frequency response
	matching is sought
p	Generic element of A and B matrices
u	Control input vector
x	State vector
y	Output vector

Greek Symbols

Presented at the 1995 American Helicopter Society Aeromechanics Specialists' Conference, Bridgeport, CT, Oct. 11-13, 1995. Manuscript submitted Nov. 1995; accepted Feb. 1997.

$\nabla^2_p(\ldots)$	Second partial derivative with respect to matrix element
ε	Frequency response error function
γ_{xy}	Coherence function
ν_o	Constant dynamic inflow component
v_s, v_c	Longitudinal and lateral dynamic inflow components
ω	Frequency in rad/sec
θ_o	Collective pitch
θ_{lc}, θ_{ls}	Lateral and longitudinal cyclic pitch
θ_t	Collective pitch of tail rotor
ζ_o	Collective lag angle
ζ _{Ic} ζ _{Is}	Longitudinal and lateral lag angle
ξ_2	Differential lag angle

Introduction

Frequency domain system identification has emerged during the last decade as a powerful tool in helicopter engineering. This technique has been used extensively to reconstruct transfer function and linear state space (i.e., stability and control derivative) mathematical models for rotorcraft flight dynamics from wind tunnel and flight test data. Compared with time domain identification, a frequency domain approach has often proved more accurate and reliable for the multi-input/multi-output problems exhibiting substantial nonlinearity, coupling, correlation, and noise that arise in many helicopter applications. Most system identification efforts based on flight test data have focused primarily on the identification of rigid-body dynamics (Refs. 1-4). A simplified treatment of main rotor dynamics and inflow dynamics has also been included, Refs. 5-7. In practice, constraints to a more sophisticated rotor identification arise from the complexity of formulating a suitable coupled rotor-fuselage model struc-

ture and from the lack of good flight test data in the frequency range of the rotor modes.

Helicopter system identification efforts have focused primarily on identifying physical quantities in a suitable differential equation model, rather than directly identifying the elements of a state space matrix representation. The former approach was applied in Ref. 8, in which the control response dynamics of a bearingless main rotor was modeled with a simplified flap-lag rigid blade formulation. The identification focused on the extraction of those values of the physical characteristics of the bearingless rotor (such as Lock number, hinge offset, flap frequency, and lift-curve slope) that would provide the best frequency response fit to the test data. On the other hand, identifying the elements of the state space matrices directly is attractive because it may reduce the required effort level of the analyst. In fact, a direct identification would only necessitate the choice of appropriate states and control inputs; it would not be necessary to establish functional relationships among them, and to choose appropriate physical parameters to identify. This, in turn, would help increase the automation of the identification process.

The state-of-the-art in helicopter applications of frequency domain system identification is such that excellent results can be obtained if care is taken while constructing the underlying mathematical model (or model structure), especially for rotor and inflow dynamics (Ref. 9). Engineering judgment is required to interpret correctly the accuracy metric information and to free or fix the model parameters appropriately during the identification. Explicit inclusion of coupled rotor-fuselage-inflow dynamics further increases both the number of model parameters to be examined and the complexity of the model identification process. Required computer processing time can also become a constraint when the identified parameter set is very large.

This paper addresses one particular aspect of frequency domain system identification, namely the calculation of state space model parameters from test data. First, a frequency response sensitivity function is defined, together with its derivatives. This function describes the sensitivity of the frequency response of a multi-input/multi-output system to a change of an element of its state or control matrix. Fully analytical expressions are used in the calculation of the sensitivity function. The sensitivity function is applied to the frequency response matching problem and to the calculation of the theoretical accuracy metrics. This results in very large computational savings compared with calculations performed using finite difference approximations.

Several additional numerical tools based on the frequency response sensitivity function are also developed. They can provide useful insight on the importance of frequency of excitation and input type on the model parameters in the identification. This information can be used to tailor the identification process. These tools can also be employed to expose potential problems or the cause of identification errors, thereby supplementing the customary examination of the theoretical accuracy metrics. Finally, the sensitivity functions are used to partition an identification problem that covers a very wide frequency band into two identifications over smaller frequency bands. A possible application of this technique is the identification of a coupled rotor-fuselage system from separate low frequency flight tests and higher frequency, rotor wind tunnel tests.

Frequency Response Sensitivity Function

Definition and Computational Aspects

The goal of frequency domain system identification is the extraction from test data or nonlinear simulation of a state space, linearized model of the helicopter that is valid for perturbed motion about a certain flight condition and over a relatively wide frequency band. High fidelity flight dynamics models are useful for control law design, simulation applications,

and nonlinear simulation validation studies. The basic state space representation of a dynamic system is

$$\dot{\mathbf{x}} = A\mathbf{x} + B\mathbf{u}$$

$$\mathbf{y} = C\mathbf{x} + D\mathbf{u}$$
(1)

where x is the system state vector, u is the control input vector, and y is the response output vector. The matrices A, B, C, and D contain the parameters that are determined in the model identification process. For a helicopter flight dynamics model, A contains the stability derivatives and B contains the control derivatives.

Frequency domain system identification compares (and iteratively matches) the frequency responses of the analytical state space model to the frequency responses obtained from test data. The frequency response matrix corresponding to Eq. 1 is given by

$$G(\omega) = C(i\omega I - A)^{-1}B + D$$
 (2)

where $G(\omega)$ is a complex-valued, three-dimensional array with a number of rows equal to the number of outputs n_o , a number of columns equal to the number of control inputs n_i , and a third dimension equal to the number n_ω of frequencies at which the match between model and test data is sought. In principle n_ω could vary for different input/output pairs, but in this study the assumption will be made that n_ω is constant for all input/output pairs used in the model identification.

The sensitivity of the frequency response function $G(\omega)$ to changes in a parameter p, where p is an element of A or B, is given by:

$$\frac{\partial G(\omega)}{\partial p} = \frac{\partial}{\partial p} [C(i\omega I - A)^{-1}B + D] \tag{3}$$

$$= C(i\omega I - A)^{-1} \frac{\partial A}{\partial p} (i\omega I - A)^{-1} B + C(i\omega I - A)^{-1} \frac{\partial B}{\partial p}$$
 (4)

assuming that C and D do not depend on p. The frequency response sensitivity function is a complex-valued, three-dimensional array with dimensions identical to those of the frequency response function $G(\omega)$. The quantity $(i\omega I - A)^{-1}$ in Eq. 4 does not depend on the parameter p, and therefore need only be calculated once per frequency; it can be stored and reused if $\frac{\partial G(\omega)}{\partial p}$ needs to be computed for more than one parameter. If the parameter p is an element of the stability derivative matrix A or of the control derivative matrix B, the derivative matrices $\frac{\partial A}{\partial p}$ and $\frac{\partial B}{\partial p}$ have a very simple structure, and contain only a "1" in the position of the element p, and zeros everywhere else.

Therefore, if p is an element of A, the second term in Eq. 4 is equal to zero. Similarly, if p is an element of B, the first term in Eq. 4 is equal to zero. The simple structure of $\frac{\partial A}{\partial p}$ and $\frac{\partial B}{\partial p}$ leads to further simplifications. Define for convenience

$$E(\omega) \doteq C(i\omega I - A)^{-1}$$
 $F(\omega) \doteq C(i\omega I - A)^{-1}B$ (5)

If p is the element (k,l) of the matrix A then the generic element (m,n) of the sensitivity matrix will be

$$\left[\frac{\partial G(\omega)}{\partial p}\right]_{mn} = E_{mk}(\omega)F_{ln}(\omega) \tag{6}$$

and if p is the element (k,l) of the matrix B

$$\left[\frac{\partial G(\omega)}{\partial p}\right]_{mn} = \begin{cases} E_{mk}(\omega) & n = l \\ 0 & n \neq l \end{cases}$$
(7)

That is, the sensitivity matrix has all its columns equal to zero, except for the l-th, which is equal to the k-th row of the $E(\omega)$ matrix. Furthermore, C is typically a diagonal matrix, and often the identity matrix, in which case

749

the calculation of $E(\omega)$ in Eq. 5 only requires N multiplications (or none at all if C = I) once $(i\omega I - A)^{-1}$ is available. The number N is equal to the size of A.

In contrast to the analytic computation, a finite difference calculation of the sensitivity matrix would yield, for the case in which p is an element of A,

$$\frac{\partial G(\omega)}{\partial p} \cong \frac{G(\omega, p + \Delta p) - G(\omega, p)}{\Delta p} \tag{8}$$

$$= \frac{1}{\Delta p} C \{ [i\omega \ I - A(p + \Delta p)]^{-1} - [i\omega \ I - A(p)]^{-1} \} B \quad (9)$$

and similarly, if p is an element of B,

$$\frac{\partial G(\omega)}{\partial p} \cong \frac{1}{\Delta p} C(i\omega \ l - A)^{-1} \left[B(p + \Delta p) - B(p) \right] \tag{10}$$

Both Eq. 9 and Eq. 10 require one additional matrix inversion per parameter at each frequency.

The frequency response sensitivity function can also be used when the parameter is not an element of the A or B matrices. For example, the parameter could be a physical constant that appears in the governing equations, and therefore affects several elements of the A or B matrices. Let q be one such parameter, and let p_p , i=1,2,...,I denote each of the elements of A and B that are functions of q. Then we have

$$\frac{\partial G(\omega)}{\partial q} = \sum_{i=1}^{I} \frac{\partial G(\omega)}{\partial p_i} \frac{\partial p_i}{\partial q}$$
 (11)

The term $\frac{\partial P_i}{\partial q}$ is the derivative of the corresponding element of A or B with respect to the parameter q. This derivative can be calculated using finite difference approximations and may even be available analytically. The term $\frac{\partial G(\omega)}{\partial p_i}$ can be calculated using Eq. 4.

The second derivative of the frequency response function $G(\omega)$ is computed by differentiating Eq. 4:

$$\frac{\partial^{2}G(\omega)}{\partial p_{j}\partial p_{k}} = C (i\omega I - A)^{-1} \frac{\partial A}{\partial p_{k}} (i\omega I - A)^{-1} \frac{\partial A}{\partial p_{j}} (i\omega I - A)^{-1} B
+ C (i\omega I - A)^{-1} \frac{\partial A}{\partial p_{j}} (i\omega I - A)^{-1} \frac{\partial A}{\partial p_{k}} (i\omega I - A)^{-1} B
+ C (i\omega I - A)^{-1} \frac{\partial A}{\partial p_{k}} (i\omega I - A)^{-1} \frac{\partial B}{\partial p_{j}}
+ C (i\omega I - A)^{-1} \frac{\partial A}{\partial p_{k}} (i\omega I - A)^{-1} \frac{\partial B}{\partial p_{k}}$$
(12)

No second derivative terms appear in Eq. 12. In fact, $\frac{\partial^2 A}{\partial p_j \partial p_k}$ and $\frac{\partial^2 B}{\partial p_j \partial p_k}$ are both zero because p_j and p_k are elements of A or B. The inverse matrix $(i\omega \ I-A)^{-1}$ is already available and need not be recalculated. The $\frac{\partial A}{\partial p_k}$ and $\frac{\partial B}{\partial p_k}$ terms in Eq. 12 also share the same structure as $\frac{\partial A}{\partial p}$ and $\frac{\partial B}{\partial p}$ terms in Eq. 4, namely, a "1" in the position of the element p_j or p_k , and zeros elsewhere. This structure can be exploited for additional computational savings.

Application to Frequency Response Matching

The starting point of a state space identification procedure is a set of frequency responses of the system to identify. This set is normally determined by applying frequency sweep type inputs (Ref. 5). The state space representation of the system to identify is given by Eq. 1. In this study we assume that the matrix D is a zero matrix and that some of the elements of A and B are known exactly, with only an estimate available for the rest. This corresponds to a model identification in which some of the model parameters have been determined very accurately, for example, from previous identifications or from simulation studies, and need not be identified.

The known elements of a model can also be physical quantities, or elements that are either "1" or "0" due to the underlying model structure. The goal of the identification, then, is to determine the unknown model parameters using the test data. The C matrix of Eq. 1 is simply used to extract the outputs y from the state vector x, and therefore is the identity matrix or a rectangular portion of it.

The unknown matrix elements in A and B are determined by matching the frequency response of the model to that from the test. This is accomplished by minimizing the objective function J, defined as

$$J = \sum_{j=1}^{n_o} \sum_{k=1}^{n_i} \sum_{l=1}^{n_w} W_{jk}(\omega_l) [\varepsilon_{jk}(\omega_l)]^2$$
 (13)

The term $\varepsilon_{jk}(\omega_l)$ represents the error between the model responses and the test frequency responses:

$$\varepsilon_{ik}(\omega_l) = G_{ik}(\omega_l) - G_{ik}(\omega_l)_{test}$$
 (14)

The function $W(\omega)$ is used to weigh the error in such a way that $W(\omega)$ varies from 1 for the best quality data (coherence function $\gamma_{xy} = 1$) to 0 for the worst (coherence function $\gamma_{xy} = 0$) (Ref. 5).

The most powerful unconstrained minimization algorithms require the gradient of the objective function J with respect to the design parameters (in this case, with respect to all the parameters p). The frequency response sensitivity function can be used to calculate the gradient of J much more efficiently than by using finite difference approximations. In fact, the derivative of J with respect to a generic design parameter p can be written as:

$$\frac{\partial J}{\partial p} = 2 \sum_{j=1}^{n_o} \sum_{k=1}^{n_i} \sum_{l=1}^{n_w} \left[\varepsilon_{jk}(\omega_l) W_{jk}(\omega_l) \frac{\partial \varepsilon_{jk}(\omega_l)}{\partial p} \right]$$
(15)

Taking the derivative of the error $\varepsilon_{ik}(\omega_l)$, Eq. 14, with respect to p yields

$$\frac{\partial \varepsilon_{jk}(\omega_l)}{\partial p} = \frac{\partial G_{jk}(\omega_l)}{\partial p} \tag{16}$$

because the test data frequency responses $G(\omega)_{lest}$ are not affected by changes in model parameters. Thus the objective function gradient can be rewritten as

$$\frac{\partial J}{\partial p} = 2 \sum_{j=1}^{n_o} \sum_{k=1}^{n_i} \sum_{l=1}^{n_w} \left[\varepsilon_{jk}(\omega_l) W_{jk}(\omega_l) \frac{\partial G_{jk}(\omega_l)}{\partial p} \right]$$
(17)

The derivative $\frac{\partial G_{jk}(\omega_l)}{\partial p}$ is the element in the *j*-th row and *k*-th column of the sensitivity function $\frac{\partial G(\omega)}{\partial p}$ given by Eq. 4. The term $\varepsilon_{jk}(\omega_l)$ need only be computed once for each gradient call, and it can be recycled for successive parameters. This further improves the efficiency of the solution process.

Application to Accuracy Metrics Calculation

After the objective function J has been minimized, two fundamental theoretical measures of accuracy, the Cramer-Rao bound and the parameter insensitivity, can be computed for each identified element (Ref. 5). The Cramer-Rao bound from a single test run establishes the standard deviation of the identified parameter; large bounds indicate poor confidence in the computed element value. Inaccuracies can result from poor data quality, correlation of parameters to identify, or improper model formulation. The parameter insensitivity quantifies the effect of each identified parameter on the objective function J and represents a lower limit on the Cramer-Rao bound. Parameter insensitivity is high when changes in the parameter do not significantly affect the objective function.

The Cramer-Rao bound, $CR_{\dot{p}}$ and parameter insensitivity, $IS_{\dot{p}}$ for each identified element p_i are approximated from the Hessian matrix H respectively as (Ref. 10):

$$CR_i \approx 2\sqrt{(H^{-1})_{ii}} \tag{18}$$

and

$$IS_i = (H_{ii})^{-1/2}$$
 (19)

where

$$H = \nabla_p^2 J \tag{20}$$

An expression for the Hessian can be obtained by taking the derivative of Eq. 15 with respect to p and neglecting higher order terms, which gives

$$H_{jk} \approx 2 \sum_{l=1}^{nw} W_{jk}(\omega_l) \left[\frac{\partial \varepsilon_{jk}(\omega_l)}{\partial p} \right]^2$$
 (21)

where the sensitivity of the local fit error $\varepsilon_{ik}(\omega_l)$ is given by Eq. 16. Note that although the sensitivity is a complex number containing amplitude and phase information, the element H_{jk} of the Hessian matrix is real. The computational savings obtained through the use of Eq. 16 and Eq. 21 are substantial, compared with the use of one-sided finite difference approximations for the calculation of $\frac{\partial \varepsilon_{ik}(\omega_l)}{\partial p}$, and even greater if central differences are used. Finite difference methods also require a check that the step size be appropriate, and may suffer from inherent phase shifts that need to be corrected. Analytic methods do not require these steps that can be time

If the parameter is not an element of the A or B matrices, then the sensitivity of the objective function J is given by:

$$\frac{\partial J}{\partial q} = \sum_{i=1}^{I} \frac{\partial J}{\partial p_i} \frac{\partial p_i}{\partial q} \tag{22}$$

where q is the parameter, and p_i , i = 1, 2, ..., I denotes the elements of A and B affected by q. The Hessian then becomes

$$H = \nabla_q^2 J = \sum_{i=1}^{I} \sum_{j=1}^{I} \frac{\partial^2 J}{\partial p_i \partial p_j} \frac{\partial p_i}{\partial q} \frac{\partial p_j}{\partial q}$$
 (23)

in which the derivatives $\frac{\partial p_i}{\partial q}$ and $\frac{\partial p_j}{\partial q}$ are the same as in Eq. 11, and the second derivative of J can be obtained very efficiently once $\frac{\partial^2 G(\omega)}{\partial p_i \partial p_j}$ is calculated to $\frac{\partial G(\omega)}{\partial p_i \partial p_j}$.

Magnitude Frequency Response Sensitivity Functions

One of the potential problems of identifying coupled rotor-fuselage models is the number of parameters that need to be identified. For larger models that are valid for a wide range of frequencies, each of the matrix elements tends to be more significant in some specific frequency band and for specific inputs. Two special forms of the frequency response sensitivity function can help provide additional information and insight on the influence of each model parameter. They will be called "magnitude" frequency response sensitivity functions because they are obtained by summing the magnitudes of the sensitivity functions in various ways.

- 1. Cumulative Frequency Response Sensitivity Function, $\frac{\partial G_{\ell}\omega}{\partial p}$ 2. Input Frequency Response Sensitivity Function, $\frac{\partial G_{\ell}(\omega)}{\partial p}$

The "cumulative" frequency response sensitivity function $\frac{\partial G_C \omega}{\partial p}$ is a real-valued vector function with one element per frequency point. The l-th element of the vector is calculated by summing the magnitudes of all the elements of $\frac{\partial G(\omega)}{\partial p}$ corresponding to the frequency ω_l , that is:

$$\frac{\partial G_C(\omega_l)}{\partial p} = \sum_{j=1}^{n_o} \sum_{k=1}^{n_i} Q_{jk} \left| \frac{\partial G_{jk}(\omega l)}{\partial p} \right| l = 1, 2, ..., n_\omega$$
 (24)

where j and k denote the matrix element in the j-th row and k-th column. The purpose of the weighting function Q is to normalize the elements of $\frac{\partial G(\omega)}{\partial n}$ when the system inputs **u** or outputs **y** are of differing units. The weighting function Q is a matrix with a number of rows equal to the number of outputs n_o and a number of columns equal to the number of control inputs n_i . Larger values of $\frac{\partial G_C(\omega)}{\partial p}$ over a specific frequency range indicate that changes in the parameter p have a greater overall impact on the responses at those frequencies.

Though the cumulative sensitivity function provides useful insight on the overall sensitivity of the frequency responses to perturbations of a parameter p, some detailed information is sacrificed by collapsing all the sensitivities into one function. For certain applications, the sensitivity of the frequency responses associated with a particular control may be of importance during the system identification process. Therefore a second, or "input," form of magnitude frequency response sensitivity function can be defined by summing at each frequency point the magnitudes of all the frequency responses corresponding to a given input. This results in a realvalued matrix function. The element of this matrix corresponding to the k-th control input and the l-th frequency is:

$$\left[\frac{\partial G_{l}(\omega)}{\partial p}\right]_{kl} = \sum_{i=1}^{n_{o}} Q_{jk} \left| \frac{\partial G_{jk}(\omega_{j})}{\partial p} \right| l = 1, 2, ..., n_{\omega}$$
 (25)

Large magnitudes of this sensitivity function for specific control input over a particular frequency range, and for a given parameter p, indicate that the identification of p is best carried out from the frequency responses to that particular control input, and in that frequency range. This information can be used to tailor the identification process by emphasizing certain control inputs and frequency bands.

The two magnitude sensitivity functions introduced in this section provide information on the sensitivity of the analytical model used in the identification to changes of its parameters. Therefore, they can be calculated independently of the test results and can provide useful information, for example, in planning the tests themselves. On the other hand, their accuracy in describing the sensitivity of the actual system will depend on the accuracy of the analytical model used in the identification. Therefore, they are best used when the primary purpose of the identification is to refine an analytical model that is already reasonably accurate.

Results

Generation of Simulated Test Data

The results of the system identification presented in this section were obtained from simulated helicopter flight test data. The time histories were generated using a linearized representation extracted from a non-linear, 4bladed, articulated rotor helicopter model consisting of a simplified version of that presented in Ref. 11. The linearization was performed in the fixed-frame about a trimmed hover flight condition, so as to obtain a coupled rotor-fuselage-inflow model in first order form. A state space simulation was chosen to generate the time history data because the use of a linear model facilitated the comparison of calculated model matrix elements with the true element values. On the other hand, no nonlinear or periodic effects were present in the simulated test data. Furthermore, the use of simulated data, even with the addition of random noise, tends to be more benign than the use of actual test data.

The bare airframe configuration used in the study was initially unstable, therefore attitude feedback loops were added in the roll and pitch channels. The additional stabilization ensured that the helicopter states returned to a trimmed flight condition after cessation of the control inputs.

The model state vector **x** contained nine fuselage, 16 rotor, and three inflow states in the fixed-frame as follows:

$$\mathbf{x} = [\mathbf{u} \ \mathbf{v} \ \mathbf{w} \ \mathbf{p} \ \mathbf{q} \ \mathbf{r} \ \mathbf{\phi} \ \mathbf{\theta} \ \mathbf{\phi} \ \dot{\mathbf{\beta}}_{1c} \ \dot{\mathbf{\beta}}_{1s} \ \dot{\mathbf{\beta}}_{2} \ \mathbf{\beta}_{0} \ \mathbf{\beta}_{1c} \ \mathbf{\beta}_{1s} \ \dot{\mathbf{\beta}}_{2}$$

$$\dot{\mathbf{\xi}}_{0} \ \dot{\mathbf{\xi}}_{1c} \ \dot{\mathbf{\xi}}_{1s} \ \dot{\mathbf{\xi}}_{2} \ \mathbf{\xi}_{0} \ \mathbf{\xi}_{1c} \ \dot{\mathbf{\xi}}_{1s} \ \dot{\mathbf{\xi}}_{2} \ \mathbf{v}_{0} \ \mathbf{v}_{s} \ \mathbf{v}_{c}]^{T}$$

$$(26)$$

The control vector was

$$\mathbf{u} = [\theta_o \, \theta_{1c} \, \theta_{1s} \, \theta_t]^T \tag{27}$$

and the outputs were

$$\mathbf{y} = [\mathbf{u} \ \mathbf{v} \ \mathbf{w} \ \mathbf{p} \ \mathbf{q} \ \mathbf{r} \ \mathbf{\phi} \ \theta \ \beta_o \ \beta_{1c} \ \beta_{1s} \ \zeta_o \ \zeta_{1c} \ \zeta_{1s} \ \zeta_2]^T \tag{28}$$

Frequency sweeps simulating flight test sweeps for each of the four control inputs (collective, longitudinal cyclic, lateral cyclic, and tail rotor) were individually computed. They were then overlaid with a computer-generated stochastic function to ensure a degree of randomness and to provide a rich spectral content over the frequency range of identification. Each control input was zero-padded for several seconds at the end of the frequency sweep allowing the helicopter to return to a trimmed flight condition. A fourth-order low-pass filter was applied to the inputs to attenuate frequencies above the range of validity of the linear model. An automated algorithm was then used to apply the resulting control inputs to the linearized helicopter state space model.

The subsequent treatment followed the process detailed in Ref. 5. Thus, a nonparametric frequency domain system identification was performed on each input/output pair. This yielded the complex-valued, three-dimensional matrix function $G(\omega)_{test}$ which consisted of the simulated test frequency responses. The chirp z-transform was used to extract high-resolution spectra in predetermined frequency bands, therefore increasing the accuracy of the identification process (Refs. 12,13). Time domain filtering, mean and trend removal, and windowing, as well as frequency domain spectral averaging, were all performed to decrease random and bias errors in the final calculations (Ref. 14). The ordinary coherence function $\gamma_{xy}(\omega)$, which is a measure of the quality of the frequency response calculations, was also computed for each frequency response.

The matrices A and B of the state space model used in this study were respectively a square matrix of size 28 and a rectangular matrix with 28 rows and four columns, for a combined total of 896 elements. For the results presented in this paper, specific numbers of the elements in A and B were freed. These elements became the design parameters of the unconstrained optimization problem. The "correct" value of each free element of A and B was assumed to be given by the corresponding element in the state space model used to generate the input and output time history data. In other words, the objective of the identification was to recover the linear model used to generate the time histories. Freeing a relatively small number of elements corresponds to an identification in which the goal might be to improve or "fine-tune" an existing model. Selection of the elements could be based on the accuracy metrics from a previous identification or a priori knowledge from simulation.

This section presents some representative results of this study. Many additional results can be found in Ref. 15.

Magnitude Frequency Response Sensitivity Function

Examples are presented here for the cumulative and control input forms of the magnitude frequency response sensitivity function, defined by Eq. 24 and Eq. 25, respectively. The output vector \mathbf{y} contained quantities with units of ft/sec, rad/sec, and radians, so the weighting matrix Q required to normalize the frequency response sensitivities used the main rotor radius to normalize lengths and rotor speed to normalize time. Because the control inputs had the same units, the columns of Q were identical, with the first column given by:

$$Q_{iI} = \begin{cases} 1/(\Omega^2 R) \ 1/(\Omega^2 R) \ 1/(\Omega^2 R) \ 1/\Omega^2 \ 1/\Omega^2 \ 1/\Omega \end{cases} 1/\Omega \ 1/\Omega \end{cases} 1/\Omega^2$$

$$(29)$$

The matching of the frequency responses was sought at a total of 90 points, logarithmically spaced between the frequencies of 0.1 and 100.0 rad/sec.

Figs. 1 through 5 and Tables 1 through 5 display results of two types of magnitude frequency response sensitivity function for several representative elements of the A and B matrices. The first four rows of Table 1 refer to the input sensitivity function $\frac{\partial G_f(\omega)}{\partial p}$, Eq. 25, for each of the four inputs. The fifth row of the table gives the values of the cumulative sensitivity function $\frac{\partial G_f(\omega)}{\partial p}$, Eq. 24. Based on the definition, the table should have 90 columns, that is one per frequency point. Instead, to summarize in a convenient way the influence of frequency and input type on the identification, the values of each of the sensitivity functions were averaged over three frequency bands, each 30 frequency points wide. The frequency bands were 0.1—1 rad/sec, 1—10 rad/sec, and 10—100 rad/sec. Thus the table has only three columns. Tables 2 through 5 were similarly obtained. A common scaling factor was used in all tables for ease of interpretation.

Fig. 1 and Table 1 refer to the element of the A matrix corresponding to the longitudinal velocity derivative X_u (without rotor and inflow contributions). The figure shows that the derivative has a greater influence on the model at frequencies below approximately 1 rad/sec. The sensitivity magnitudes decrease rapidly at higher frequencies, indicating that changes to this element have a smaller impact on the model at frequencies above about 1 rad/sec. Because X_u affects primarily the rigid-body modes of the helicopter, changes to its value do not significantly alter the precision of the state space model at higher frequencies. Fig. 1 also shows that longitudinal cyclic is the dominant control input for X_u , especially for frequencies between 0.1 rad/sec and 3 rad/sec. These results imply that the derivative X_u is best identified through the frequency response to a longitudinal cyclic input at frequencies between 0.1 and 1 rad/sec.

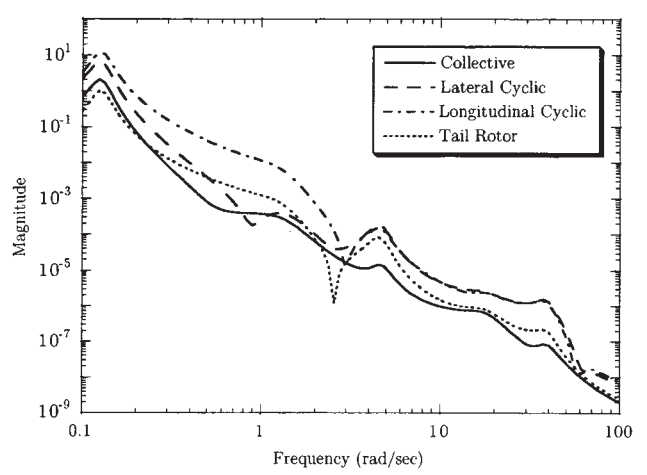


Fig. 1. Input frequency response sensitivity functions for longitudinal velocity derivative $X_u = A_{11}$.

Table 1. Input and Cumulative Sensitivity Functions for Longitudinal Velocity Derivative $X_u = A_{11}$

Frequency (rad/sec) →	0.1-1	1-10	10-100
Collective	9.2219	0.0026	0.0000
Lateral Cyclic	29.2817	0.0042	0.0001
Longitudinal Cyclic	56.7452	0.0558	0.0000
Tail Rotor Collective	4.6820	0.0064	0.0000
Cumulative	99.9309	0.0690	0.0001

Fig. 2 and Table 2 refer to the element of the A matrix corresponding to the yaw damping derivative N_r . Yaw damping is mainly a rigid-body mode and therefore has a greater impact on the model fidelity at low frequencies. Fig. 2 shows that the cumulative magnitude frequency response sensitivity is higher for frequencies less than approximately 5 rad/sec and rolls off for higher frequencies. This figure also shows that the largest contribution is that due to the tail rotor input. Therefore, the derivative N_r is best identified through the frequency response to a tail rotor input at frequencies between about 0.1 and 5 rad/sec.

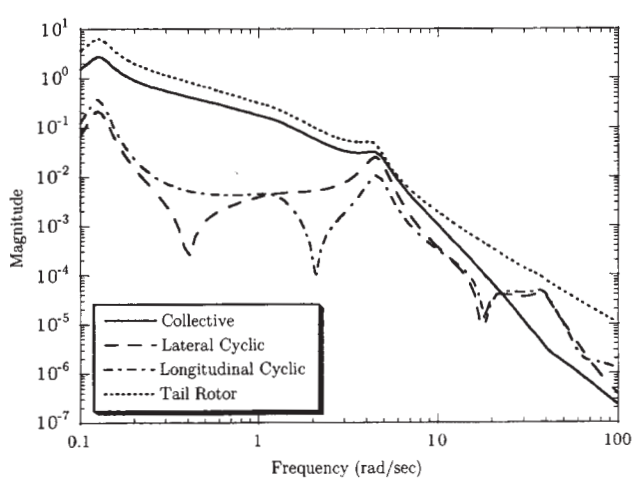


Fig. 2. Input frequency response sensitivity functions for yaw damping derivative $N_r = A_{66}$.

Table 2. Input and Cumulative Sensitivity Functions for Yaw Damping Derivative $N_r = A_{66}$

		7	
Frequency (rad/sec) →	0.1-1	1-10	10-100
Collective	28.6459	1.7186	0.0036
Lateral Cyclic	1.1094	0.2283	0.0017
Longitudinal Cyclic	1.8909	0.0926	0.0018
Tail Rotor Collective	63.3886	2.9082	0.0106
Cumulative	95.0348	4.9476	0.0176

The sensitivity results for the element (10,14) of the A matrix are presented in Fig. 3 and Table 3. This is the element in the row of A corresponding to the derivative $\dot{\beta}_o$ and in the column corresponding to β_o . For convenience this element is referred to as $\dot{\beta}_o/\beta_o$. A similar nomenclature is used for other elements of the A and B matrices. The collective flap element $\dot{\beta}_o/\beta_o$ is a rotor parameter and has an impact on the rotor model at mid and high frequencies as seen in Fig. 3. The cumulative magnitude sensitivity function is relatively flat for frequencies below approximately 30 rad/sec. This plot also shows that perturbations of the the collective flap parameter $\dot{\beta}_o/\beta_o$ impact significantly the frequency response to collective pitch, while having a much smaller effect on the responses to remaining

three control inputs. Table 3 confirms these results by indicating that the cumulative sensitivity function values are relatively even for the three frequency bands used in the calculations, and that the largest contribution comes from the sensitivity of the collective pitch. This behavior implies that the identification of the element $A_{10,14}$ is best accomplished from frequency responses to collective pitch inputs, and that the frequency of excitation is relatively unimportant.

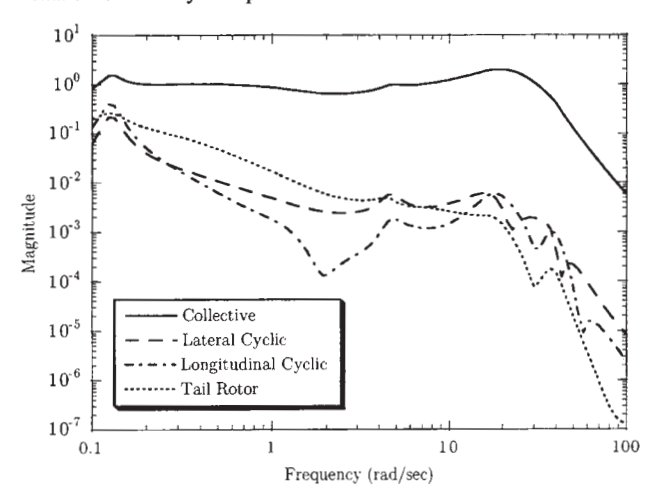


Fig. 3. Input frequency response sensitivity functions for collective flap parameter $\beta_o/\beta_o = A_{10,14}$.

Table 3. Input and Cumulative Response Sensitivity Functions for Collective Flap Parameter $\dot{\beta}_o/\beta_o = A_{10.14}$

10. 00.00.00	· · · · · · · · · · · · · · · · · · ·	PO-PO	0,14
Frequency (rad/sec) →	0.1-1	1-10	10-100
Collective	34.8967	27.6203	29.3957
Lateral Cyclic	1.5225	0.1148	0.0648
Longitudinal Cyclic	2.3804	0.0296	0.0547
Tail Rotor Collective	3.5216	0.1969	0.0250
Cumulative	42.3211	28.1385	29.5404

The sensitivity results for the element $A_{19,16}$ are presented in Fig. 4 and in Table 4. This element can be defined as a coupled longitudinal lag/lateral flap parameter $\dot{\xi}_{1c}/\beta_{1s}$. The cumulative sensitivity function is low at frequencies below approximately 1 rad/sec and is larger at frequencies above this value. The parameter $\dot{\xi}_{1c}/\beta_{1s}$ is part of the main rotor portion of the helicopter model. Therefore it has less effect on the rigid-body dynamics, but needs to be included when the rotor dynamics is to be identified. For frequencies above approximately 1 rad/sec, Fig. 4 indicates that perturbations of $\dot{\xi}_{1c}/\beta_{1s}$ have the strongest influence on frequency responses to lateral cyclic input and, to a smaller extent, to longitudinal cyclic. The lateral and longitudinal cyclic sensitivity function values are the largest of the four controls presented in Table 4 for the frequency range 1-100 rad/sec. This implies that the element $A_{19,16}$ is best identified from frequency responses to lateral cyclic, or to a lesser extent longitudinal cyclic, at frequencies between 3-4 and 30-40 rad/sec.

Finally, Fig. 5 and Table 5 present the sensitivity results for the element $B_{11,2}$ of the control matrix B, corresponding to the uncoupled parameter β_{1c}/θ_{1c} . Because this parameter is an element of the control derivative matrix B, the input frequency response sensitivity function contains only data for θ_{1c} and zeros for the other control inputs. This explains the zero rows in Table 5 and the presence of just one curve in Fig. 5. The sensitivity results indicate that $B_{11,2}$ is best identified below 10 rad/sec, and especially in the frequency bands around the two resonance peaks, that is around 0.1-0.3 and 2-7 rad/sec.

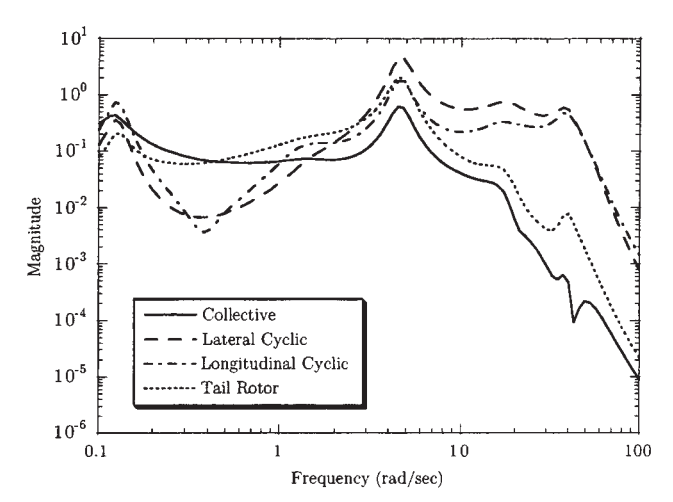


Fig. 4. Input frequency response sensitivity functions for coupled longitudinal lag/lateral flap parameter $\dot{\xi}_{1c}/\beta_{1s}=A_{10,14}$.

Table 4. Input and Cumulative Sensitivity Functions for Coupled Longitudinal Lag/Lateral Flap Parameter $\dot{\xi}_1/\beta_{1s}=A_{19.16}$

			91071819,16
Frequency (rad/sec) →	0.1-1	1-10	10-100
Collective	4.6952	5.0600	0.2741
Lateral Cyclic	1.9141	31.4410	12.4763
Longitudinal Cyclic	3.8658	13.9107	7.0905
Tail Rotor Collective	3.0870	15.5644	0.6208
Cumulative	13.5621	65.9762	20.4617

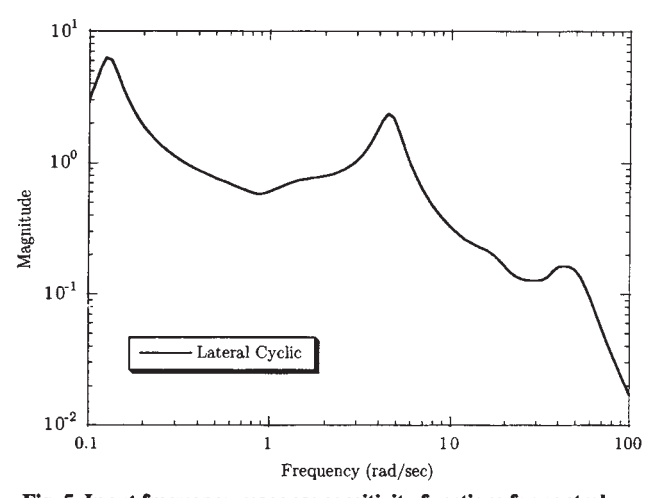


Fig. 5. Input frequency response sensitivity functions for control derivative $\beta_{1c}/\theta_{1c}=B_{11,12}$.

Table 5. Input and Cumulative Sensitivity Functions for Control Derivative β_{1o}/θ_{1s}

Frequency (rad/sec) →	0.1-1	1-10	10-100
Collective	0.0000	0.0000	0.0000
Lateral Cyclic	62.7058	32.5182	4.7759
Longitudinal Cyclic	0.0000	0.0000	0.0000
Tail Rotor	0.0000	0.0000	0.0000
Cumulative	62.7058	32.5182	4.7759

In summary, the examples presented in Figs. 1 through 5 and Tables 1 through 5 indicate that the magnitude sensitivity functions can be a useful tool in the planning and interpretation of a system identification procedure, and that the quantitative information that they provide agrees with engineering judgment. This suggests that the use of such functions can help increase the automation of some parts of the identification process or, equivalently, reduce the level of training required of the analyst performing the identification.

Frequency-Banded State Space Identification

This section presents the results of a complete state space identification for the coupled rotor-fuselage system. The Broyden-Fletcher-Goldfarb-Shanno (BFGS) algorithm for unconstrained optimization, Ref. 16, was used to minimize the performance index J defined in Eq. 13. Two types of identification were conducted. For the first type, which represents the baseline solution, a total of 40 elements from both the A and B matrices were identified simultaneously over the entire frequency range from 0.1 to 100 rad/sec. It should be noted that the mode with the lowest frequency was the phugoid, at 0.12 rad/sec, whereas that with the highest was the collective flap, at 50.84 rad/sec. The elements to be identified included stability and control derivatives from both the rotor and fuselage portions of the model, as well as from portions of the state matrix A that couple rotor and fuselage dynamics. The second type of cases were studied to determine the feasibility of performing the parameter identification in a piecewise way. This was done by identifying some of the unknown elements of A and B in one frequency band, and the rest in a different frequency band, based on the information generated by the frequency response sensitivity functions. In the remainder of the section, this type of identification will be called "frequency-banded." In both types of cases the initial guess for the 40 elements to identify was obtained by multiplying the known correct values (that is, those used in the calculation of the simulated test data) by a random vector with a uniform distribution.

For the frequency-banded identification method, the 40 elements were partitioned into two groups using the cumulative frequency response sensitivity function, Eq. 24. Nineteen elements, primarily from the fusclage portions of the state space model, were found to be most significant in the frequency range 0.1-10 rad/sec, while the remaining 21 elements had more impact on the model frequency responses for frequencies between 5 and 100 rad/sec. The identification was performed in two steps. In the first, the 21 "high frequency" elements were freed, while the remaining 19 "low frequency" elements were kept fixed at their respective initial (and incorrect) solution guess. The 21 free elements were identified using only data in the frequency range of 5-100 rad/sec. In the second step, the 21 high frequency elements were held fixed at their respective identified value and the 19 low frequency elements were freed. These low frequency elements were identified using only data in the 0.1-10 rad/sec frequency range. The same amount of frequency response data was used in the baseline case and in the high and low frequency identifications of the frequency-banded case.

Table 6 shows the required CPU time and the error performed in both types of identification. The accuracy of the prediction of the poles was chosen as an overall measure of the accuracy of the entire identification. The CPU time shown for the frequency-banded identification was the sum of the times required for the high frequency identification and for the low frequency identification. The rotor and fuselage pole error data represent the average of the relative errors for all the poles in the respective portion of the model. The average pole error for all the identified poles for the baseline case was 3.24%, indicating a good overall accuracy of the identification. The fuselage pole error was typically slightly larger than the rotor pole error due mainly to some numerical problems in the identification of the low frequency rigid-body modes in hover. The rigid-body derivatives were normally much smaller than many of the rotor derivatives, and this

numerical difference appears to be the main cause of the slightly larger inaccuracies in the "fuselage" poles predictions.

For the frequency-banded identification case, the errors in the determination of the poles decreased slightly. Identification of the rigid-body poles in general was more sensitive to errors in the matrix elements than identification of the main rotor poles due to the higher coupling of the fuselage modes in hover. The frequency-banded identification method also yielded a 41% reduction in required CPU time as compared to the baseline case. The savings in CPU time resulted from a smaller parameter set to identify in each of the high and low frequency bands as compared to the identification of the complete set of 40 parameters for the baseline case. The accuracy of the frequency-banded identification was found to be rather sensitive to the proper choice of frequency bands and of the free parameters. Table 6 shows the results of one of the most accurate identifications.

Table 6. Comparison of CPU Time and

Average Life in the identified roles				
	CPU Time	Average Pole Error		
Method	(Minutes)	Rotor	Fuselage	Total
Baseline	160	1.58%	6.56%	3.24%
Frequency-Banded	94	1.17%	5.89%	2.75%

Verification in the time domain was conducted after each test case by supplying a control input, different from that used for the identification, to both the identified model and the model used to generate the simulated flight test data. For all controls, this input consisted of a rectangular pulse of 3.5 seconds started at time t = 1 sec. The rectangular shape of the input has to be considered as a mathematical idealization. In reality it would be impossible to achieve the instantaneous changes at the beginning and the end of the input that such shape implies. Figs. 6 through 9 are representative of the results of the validation. They show respectively the response of the fuselage pitch attitude to collective pitch, of the fuselage pitch rate to lateral cyclic, of the lateral lag angle of the rotor to lateral cyclic, and of the longitudinal lag angle of the rotor to longitudinal cyclic. Each figure contains three curves. The curve marked "Correct" denotes the simulated test data. The curve marked "Baseline ID" shows the response obtained from the baseline identification. Finally, the curve marked "Frequency-Banded ID" shows the response of the state space system obtained following the frequency-banded identification process. The figures confirm

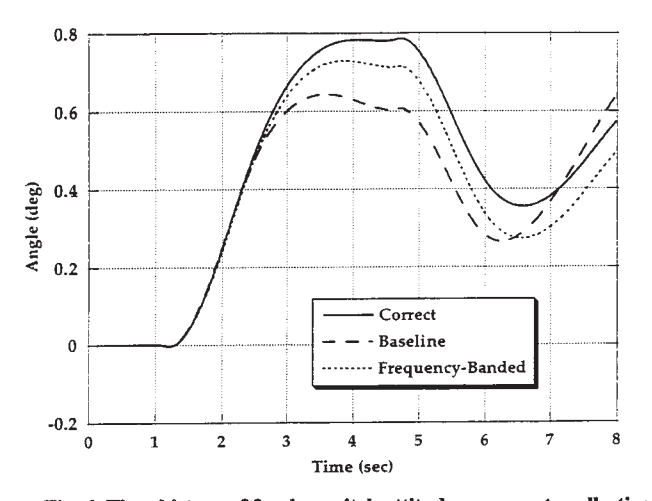


Fig. 6. Time history of fuselage pitch attitude response to collective input.

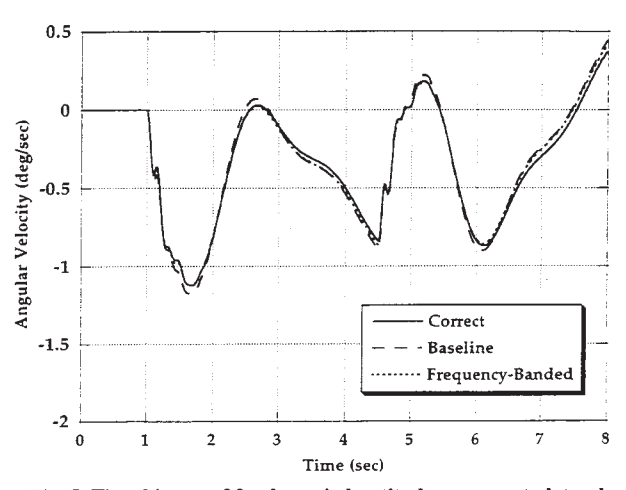


Fig. 7. Time history of fuselage pitch attitude response to lateral cyclic input.

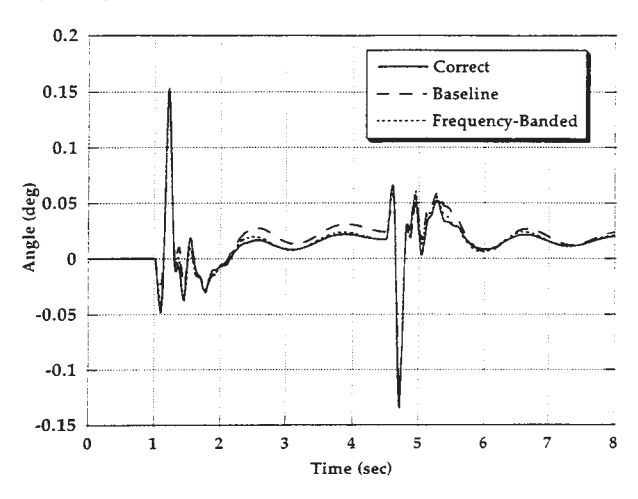


Fig. 8. Time history of rotor lateral lag angle response to lateral cyclic input.

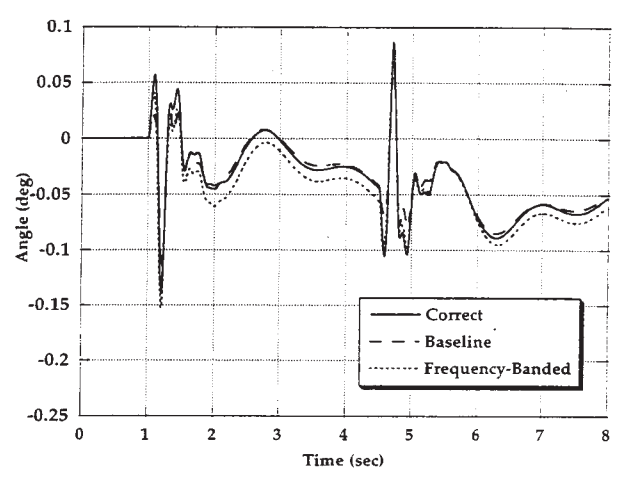


Fig. 9. Time history of rotor longitudinal lag angle response to longitudinal cyclic input.

that the frequency partitioning of the identification does not compromise the accuracy of the results; for several input-output pairs the frequencybanded identification even appears to be more accurate than the baseline.

The primary objective in defining a frequency-banded identification process was to determine whether an identification over a very wide frequency band could be partitioned into two (or possibly more) identifications over smaller frequency bands. The results shown in this section indicate that this may indeed be possible. The results also show that the procedure may be faster, and also yield improvements in accuracy.

Computational Efficiency Comparison

Fig. 10 shows a comparison of the CPU time required to calculate the frequency response sensitivity function $\frac{\partial G(\omega)}{\partial p}$ using different computational schemes and assumptions. The comparisons were conducted using Fortran with full compiler optimization on a Sun Sparc5 workstation. The bar marked FD indicates the time required when finite difference approximations were used to calculate the gradients. The three bars marked A indicate the times required using the analytical formulation presented in this study. The A1 bar refers to a direct application of Eq. 4. The CPU time of bar A2 was obtained by exploiting the mathematical structure of $\frac{\partial A}{\partial p}$ and $\frac{\partial B}{\partial p}$ (see Eqs. 5 through 7). Finally, for bar A3 the additional assumption was made that the C matrix was either the identity matrix or a portion of it, so that its function was merely to select specific elements of the state vector. The case in which the C matrix is a diagonal matrix or a rectangular portion of it, but not the identity matrix, was not explicitly considered but should yield CPU times very close to that of case A3. The results shown in Fig. 10 indicate that the analytical formulation of the present study reduces the computer time required for the calculation of $\frac{\partial G(\omega)}{\partial p}$ by an amount that ranges from 39% to 97% compared with the case in which finite differences are used. These figures refer to the example of the present study, with a state matrix A of size 28 and 40 free parameters to be identified. The CPU times savings were mostly due to the fact that a matrix of the size of A needs to be inverted only once per frequency value, rather that once per free parameter. Therefore the savings will increase with the size of the mathematical model (which determines the cost of inverting a matrix of the size of the state matrix A) and with the number of free parameters (which determines the number of matrix inversions at each frequency).

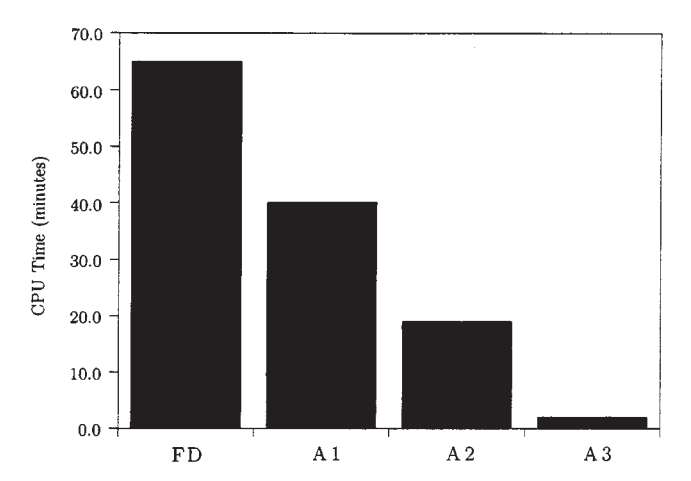


Fig. 10. Comparison of required CPU time for frequency response sensitivity function calculation (FD: Finite Difference methods; A1, A2, A3: Analytic methods of this study).

Fig. 11 presents a comparison of the CPU time required to complete the model identification and parameter accuracy metric calculations for frequency response sensitivities calculated numerically and analytically. For the numeric method, the BFGS optimization algorithm used one-sided finite-difference approximations to the gradients for each freed element. Central-difference methods were used to compute the Cramer-Rao bound and parameter insensitivity percentages. Three separate cases using the analytic frequency response sensitivities to compute both the objective function gradients and the theoretical accuracy metrics were also executed. These three cases were identical to those described in Fig. 10.

The baseline numeric calculations required a total of 585 minutes, of which 520 minutes was used for the model identification and 65 minutes was used for the theoretical accuracy metrics calculation (bar marked "FD" in Fig. 10). Introduction of the frequency response sensitivity function with no other assumptions made on the model structure reduced the CPU time to 464 minutes for the model identification and 40 minutes for the accuracy metrics calculation, a total decrease of approximately 14% (bar marked "A1" in Fig. 11). With the assumptions made on the structure of the A and B matrix derivatives, the total required CPU time was reduced further to 319 minutes, which was a decrease of approximately 46% as compared to the baseline numeric results (bar marked "A2" in Fig. 11). Incorporation of the final assumption on the structure of the output matrix C yielded a total required CPU time reduction of approximately 72% to 162 minutes (bar marked "A3" in Fig. 11).

The values of the identified elements were identical for all three of the analytic test cases. The difference between the values identified using finite difference methods and those identified using analytic methods was less than 1% for each element. The small error is due to the accuracy of the analytic gradients computed using Eq. 15 as compared to the gradients computed internally by the optimization algorithm.

Although they are quite substantial, the improvements in required CPU time for the complete identification shown in Fig. 11 were smaller than those obtained for the frequency response sensitivity function $\frac{\partial G(\omega)}{\partial p}$ shown in Fig. 10. This was mostly due to the following reason. The BFGS algorithm, like most optimization methods, consists of repeatedly applying two basic steps: (i) the determination of a direction of the design space along which the objective function decreases, and (ii) a one-dimensional minimization of the objective function along that descent direction. The direction finding step requires the calculation of the gradient of the objective function, and it is in the execution of this step that the majority of the computational efficiency is gained when using the expression for $\frac{\partial G(\omega)}{\partial p}$ presented in this paper. On the other hand, the one-dimensional minimization step requires the calculation of the objective function, but not of its gradient. Therefore no computational gains were obtained using the methods of this paper for this portion of the optimization. Since both first and second derivatives of the objective function J can be calculated efficiently using the first and second derivatives of the frequency response, Equations 4 and 12, it is possible to build second order Taylor series expansions of J in terms of the parameters p to be identified. Then the one-dimensional minimization steps could be performed on the Taylor series approximations rather than on the original objective function J. This technique was not attempted in the cases presented in this paper, but has the potential for further substantial reductions of required computer time.

Summary and Conclusions

This paper focused on some aspects of the frequency domain based system identification of a large dynamic system, such as a coupled rotor-fuselage helicopter model, described in state-space form. The case of interest was one in which some elements of the state and control matrices

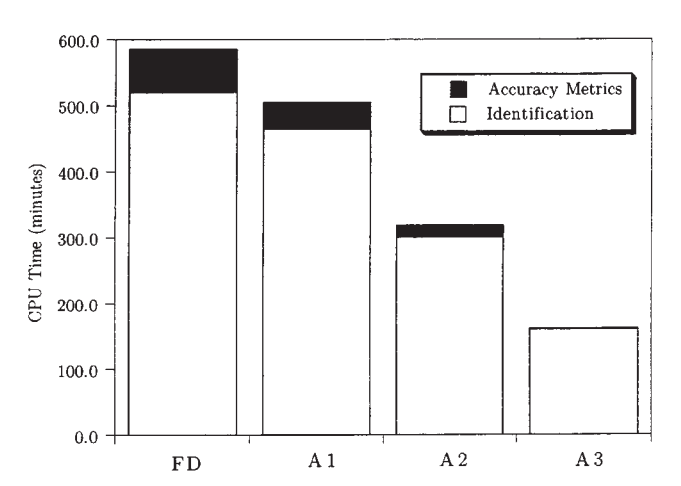


Fig. 11. Comparison of required CPU time for state-space identification and accuracy metrics calculation (FD: Finite Difference sensitivities; A1, A2, A3: Analytic sensitivities).

are identified directly. The identifications were performed using simulated test data obtained from a linearized model in hover: these limitations should be kept in mind when generalizing all the results and conclusions of this study.

A frequency response sensitivity function, which describes the sensitivity of the frequency responses of a linear system to changes in elements of the state and control matrices was defined, and analytical expressions for its derivatives were obtained. These expressions allow an efficient use of powerful, gradient based numerical optimization methods in the frequency matching part of the system identification. These expressions can also be used for an efficient calculation of the accuracy metrics. The results show substantial efficiency gains compared with the cases in which finite difference approximations are used to calculate derivative information.

Modifications of the frequency response sensitivity function were found to be useful in determining which types of inputs, and over which frequency bands, are the best for the identification of a given element of the state or the control matrix. These functions provided quantitative results consistent with engineering judgment, and thus can help automate some critical phases of the system identification. These expressions provide valuable information on the interaction of the model parameters and can be employed to tailor the identification process.

It appears possible to partition an identification that requires a wide frequency band into two or more identifications that can be performed over smaller frequency bands. The specific parameters to be identified in each of the subproblems can be selected using the magnitude sensitivity functions described in the paper. Partitioning the identification also reduces the computational requirements, and may improve the overall accuracy of the identification. A possible application of this technique is the identification of a coupled rotor-fuselage system from separate low frequency flight tests and higher frequency, rotor wind tunnel tests.

Acknowledgments

The authors acknowledge the support for this research work by the Army Research Office under the Center for Rotorcraft Education and Research contract DAAH-04-94-G-0074; Technical Monitor Dr. Tom Doligalski.

References

¹Fletcher, J.W., "Identification of UH-60 Stability Derivative Models in Hover from Flight Test Data," *Journal of the American Helicopter Society*, Vol. 40, (1), Jan 1995.

²Tischler M.B., "Advancements in Frequency Domain Methods for Rotorcraft System Identification," *Vertica*, Vol. 13, (3), 1989.

³Ballin, M.G., and Dalang-Secrétan, M., "Validation of the Dynamic Response of a Blade-Element UH-60 Simulation Model in Hovering Flight," *Journal of the American Helicopter Society*, Vol. 36, (4), Oct 1991.

⁴Ham, J.A., Gardner, C.K., and Tischler, M.B., "Flight-Testing and Frequency-Domain Analysis for Rotorcraft Handling Qualities," *Journal of the American Helicopter Society*, Vol. 40, (2), Apr 1995.

⁵Tischler, M.B., and Cauffman, M.G., "Frequency-Response Method for Rotorcraft System Identification: Flight Applications to BO 105 Coupled Rotor/Fuselage Dynamics," *Journal of the American Helicopter Society*, Vol. 37, (3), Jul 1992.

⁶Fu, K.-H., and Kaletka, J., "Frequency-Domain Identification of BO 105 Derivative Models with Rotor Degrees of Freedom," *Journal of the American Helicopter Society*, Vol. 38, (1), Jan 1993.

⁷Fu, K.-H., and Kaletka, J., "BO 105 System Identification for Hover Flight Condition," Nineteenth European Rotorcraft Forum, Cernobbio, Italy, Sep 1993.

⁸Tischler, M.B., Driscoll, J.T., Cauffman, M.G., and Freedman, C.J., "Study of Bearingless Main Rotor Dynamics from Frequency-Response Wind Tunnel Test Data," AHS/NASA Aeromechanics Specialists Conference, San Francisco, CA, Jan 1994.

⁹Houston, S.S., and Black, C.G., "Identifiability of Helicopter Models Incorporating Higher-Order Dynamics," *AIAA Journal of Guidance, Control, and Dynamics*, Vol. 14, (4), Jul 1991.

¹⁰Maine, R.E., and Iliff, K.W., "The Theory and Practice of Estimating the Accuracy of Dynamic Flight-Determined Coefficients," NASA RP-1077, Jul 1981.

¹¹Kim, F.D., Celi, R., and Tischler, M.B., "Forward Flight Trim Calculation and Frequency Response Validation of a High-Order Helicopter Simulation Model," *Journal of Aircraft*, Vol. 30, (6), Nov 1993.

¹²Rabiner, L.R., Schafer, R.W., and Rader, C.M., "The Chirp z-Transform Algorithm and Its Application," *The Bell System Technical Journal*, May 1969.

¹³Rabiner, L.R., "Chirp z-Transform Algorithm Program," *Programs for Digital Signal Processing*, Edited by Digital Signal Processing Committee, The IEEE Press, Inc., 1979, pp. 1.6-1–1.6-13.

¹⁴Bendat, J.S., and Piersol, A.G., Random Data Analysis and Measurement Procedures, 2nd Edition, John Wiley & Sons, Inc., New York, 1986, pp. 361–418.

¹⁵Jones, C. T., "Contributions to Helicopter Frequency Domain System Identification," Ph.D. Dissertation, Department of Aerospace Engineering, University of Maryland, College Park, MD, Feb 1997.

¹⁶Vanderplaats, G.N., *Numerical Optimization Techniques for Engineering Design: With Applications*, McGraw-Hill Book Co., New York, 1984, pp. 92—93.

The authors

Christopher Tyler Jones Sikorsky Aircraft Corporation, 6900 Main Street, Mail Stop S317A, Stratford, Connecticut 06615 (ctjones@sikorsky.com). Dr. Jones earned an undergraduate degree in aerospace engineering from the Georgia Institute of Technology in 1986, a master's degree in aerospace engineering, a second master's degree, in engineering management, from the University of Dayton in 1991, and a Ph.D. in rotorcraft flight mechanics from the University of Maryland in 1997. This paper was written while he was at the University of Maryland. In June 1996, he joined the Aeromechanics Group at Sikorsky Aircraft, where he has supported design and development of active noise systems, active vibration systems, and rotor systems for tiltrotor applications. Dr. Jones is also a Major in the Connecticut Air National Guard.

Roberto Celi Department of Aerospace Engineering, University of Maryland, College Park, Maryland 20742 (celi@eng.umd.edu). Dr. Celi received a B.S. degree in aeronautical engineering from the Politècnico di Torino, Italy, and M.S. and Ph.D. degrees in aerospace engineering from the University of California, Los Angeles, in 1982 and 1987, respectively. Since 1987 he has been a faculty member in the Department of Aerospace Engineering at the University of Maryland, where he is an Associate Professor, and where he is also a member of the Alfred Gessow Rotorcraft Center. His research interests, all centered on rotorcraft, include flight dynamics and handling qualities, rotor dynamics and aeroelasticity, and multidisciplinary design optimization.

Publication of this paper

This paper was originally published on pages 244–253 of the *Journal of the American Helicopter Society*, Volume 42, Number 3 (1997) [Copyright © 1997 by the American Helicopter Society. All rights reserved.]. It was produced by scanning the original version and contains added biographical sketches of its authors. We gratefully acknowledge permission to include it in this issue.